The influence of N-methylation on the ansamers of an amatoxin: Gly5Sar-amanullin

Marius T. Wenz,[†] Simone Kosol,[‡] Guiyang Yao,[¶] Roderich D. Süssmuth,[‡] and Bettina G. Keller[*,†]

†*Freie Universität Berlin, Department of Biology, Chemistry and Pharmacy, Arnimallee 22, 14195 Berlin, Germany.*

‡*Technische Universität Berlin, Institute for Chemistry, Strasse des 17. Juni 124, 10623 Berlin, Germany.*

¶*Fudan University, Center for Innovative Drug Discovery, Greater Bay Area Institute of Precision Medicine (Guangzhou), School of Life Sciences, PR China.*

E-mail: bettina.keller@fu-berlin.de

Abstract

Amatoxins are strong inhibitors of RNA polymerase II, and cause cell death. Because of their cytotoxicity they are candidates for anti-cancer drugs, and understanding their structure-activity relationship is crucial. Amatoxins have a rigid bicyclic scaffold which consists of a cyclic octapeptide bridged by cysteine and tryptophan side chain forming a tryptathionine bridge. Here we show the influence of the N-methylation on the amatoxin scaffold by studying Gly5Sar-amanullin with MD simulations and NMR experiments. Since we have shown recently that the amatoxin scaffold allows for two isomeric forms (ansamers), we studied both isomers of Gly5Sar-amanullin. We found that both isomers of Gly5Sar-amanullin form two long-living conformations which is unusual for amatoxins, and that they are differently affected by the N-methylation. The natural

Gly5Sar-amanullin forfeits the hydrogen bonds to Gly5 due to the N-methylation, which is expected from existing crystal structures for alpha-amanitin. Our results however indicate that this does not cause more flexibility due to a shift in the hydrogen bond pattern. In the unnatural isomer, we observe an interesting cis-trans-isomerisation of the backbone angles in Trp4 and Gly7, which is enabled by the N-methylation. We expect that our perspective on the effect of N-methylation in amatoxins could be a starting point for further SAR-studies which are urgently needed for the design of better anti-cancer agents.

Introduction

Amatoxins are a family of "utterly powerful poisons"[1] that occur in several poisonous mushrooms, most-notably the death cap mushroom (*Amanita phalloides*).[2–6] They consist of eight amino acids with the general sequence Asn-Pro-Ile-Trp-Gly-Ile-Gly-Cys which are joined in a cyclic peptide chain (macrolactam). Additionally, amatoxins have a covalent bridge between cysteine and tryptophan (tryptathionine bridge), such that their overall structure is a bicyclic octapeptide. The various members for the amatoxin family differ in the hydroxylation and amination of residues Asp1, Pro2, Ile3, and Trp4.[2] The most prominent member of this family is α-amanitin.[7]

Amatoxins are stable at temperatures beyond 100 °C and thus cannot be destroyed by cooking the poisonous mushrooms. They are water-soluble which facilitates their oral uptake. Finally, their exceptional structure makes them resistant against stomach acid or digestion by proteases.[2,3,8] They act by inhibiting RNA polymerase II, thereby shutting down protein synthesis and cell metabolism.[9–12] By interacting with cell membranes, amatoxins can also be responsible for cell lysis and misplaced cell organelles.[2] Amatoxins can affect all organs, but their effect on liver and heart is most destructive, and a fatally poisoned animal or human usually dies of liver or heart failure.[13–15] No definitive antidote is available, and, in case of liver failure, a liver transplant is the only viable treatment.[5,15]

Because amatoxins are so extraordinarily cytotoxic, they are ideal candidates for targeted anti-cancer therapy.[16,17] In this approach, one develops an antibody that binds to an antigen on the surface of the cancer cell and couples it to a potent cytoxin. After uptake by the cancer cell, the cytoxin is cleaved from the antibody, and the released cytotoxin kills the cancer cell.

Even though amatoxins are very promising payloads for antibody-drug conjugates,[16,18] they could not be used in cancer research until recently, because their synthesis is extremely challenging. In mushrooms, amatoxins are ribosomally synthesised,[4,19] but obtaining amatoxins in sufficient quantity and quality from mushroom farms proved to be impossible.[16,20,21]

Until today, there have only been four reports on the successful synthesis of α-amanitin, all of which were published in the last five years.[20,22–24] We recently proposed a very efficient synthesis for amatoxin,[24] which allowed us to build an amatoxin library to systematically study their structure-activity relationship.[25]

Each amatoxin can in principle occur as two different isomers, which differ in the position of the tryptathionine bridge relative to the macrolactam ring. Here, the two sides of the macrolactam ring are defined by the direction of peptide chain: NH $\rightarrow$ C_α $\rightarrow$ CO. When looking down on the macrolactam ring and the peptide chain proceeds clock-wise, one looks at the "upper side" of the ring. So far, only the isomer, in which the bridge is located above the macrolactam ring has been isolated from mushrooms.

The existence of the second isomer, in which the tryptathionine bridge is below the macrolactam ring, was highly debated in literature.[26–28] However, recently we were able to synthesise, isolate and characterise both isomers of the amatoxin amanullin.[29] We also proposed the term 'ansamers' for this particular isomerism, where P_{ansa} is the natural isomer with the bridge above the macrolactam ring, and M_{ansa} is the newly synthesized non-natural isomer with the bridge below the macrolactam ring. Formally, the two ansamers can be interconverted by rotating the tryptathionine bridge around the (imaginary) axis between the two bridgeheads, but this rotation is hindered by the macrolactam ring. Consequently, the ansamers are in fact two separate substances, which differ in their structure and physicochemical properties. For example, the M-ansamer of amanullin has a different intramolecular hydrogen-bond pattern which makes it more compact and more hydrophobic than the P-ansamer.

Monocyclic peptides often exhibit a variety of conformations which differ in their physicochemical properties and interconvert on relatively slow timescales, often microseconds or slower[30–33] However, the interconversion is usually not slow enough to separate the conformations by chromatography or similar techniques. Yet, the conformational dynamics are crucial for understanding and tuning the structure-activity relationship of monocyclic

peptides.[28,30,31,34,35] A classic example is cyclosporine which can interconvert between a hydrobphilic conformation which facilitates oral uptake, and a hydrophobic conformation which facilitates membrane permeation.[36–39] With this in mind, two questions arise: (1) Can amatoxins exhibit several conformations, or does the tryptathionine bridge enforce one dominant conformation? (2) How do the conformations differ in the *P*-ansamer and in the *M*-ansamer?

In our previous study, we studied amanullin which differs from α-amanitin in the hydroxylation of the side chains in position 4 and 6. At position 4, it contains a normal tryptophan instead of the hydroxylated 6-OH-tryptophan (OHTrp), and at position 6, it contains a normal isoleucine instead of the twice hydroxylated (3*R*,4*R*)-4,5-dihydroxyisoleucine (DHIle). Spectroscopic data indicated that amanullin only forms a single dominant backbone conformation in each of the ansamers of amanullin (with two conformations of the Ile3-ethyl group in the crystal structure of the *M*-ansamer).[29] The conformation of the *P*-ansamer is stabilized by a strong hydrogen bond from the amide of Gly5 to the carbonyl oxygen of Asn1. This hydrogen bond is known to contribute to the overall rigidity of the amatoxin scaffold.[29,40,41]

Here, we investigate the amatoxin Gly5Sar-amanullin, in which the amide of Gly5 has been methylated (sarcosine), thereby prohibiting the stabilizing hydrogen bond. N-methylation is a well-established strategy to modify the structure and dynamics of monocyclic peptides.[42,43] We combine classical molecular dynamics (MD) simulations of the *P*-ansamer and *M*-ansamer of Gly5Sar-amanullin with NMR experiments of the *M*-ansamer to identify the stable conformations of Gly5Sar-amanullin. We show that the methylation has a very different affect on the *P*-ansamer than on the *M*-ansamer.

Results and discussion

Gly5Sar-amanullin

The conformation of α-amanitin and P_{ansa}-amanullin is stabilized by a hydrogen bond between the amide hydrogen of Gly5 and the backbone carbonylgroup of Asn1 (Figure 1.c).[29] This hydrogen bond is also found in the crystal structures of other amatoxins.[44] To investigate the effects of the loss of this hydrogen bond on the structure and conformational stability, we synthesized a derivative with the N-methylated amino acid sarcosine (three-letter code: Sar) instead of glycine 5 (Figure 1.b).

Ansamers arise in bicyclic structures in which at least one of the cycles has a clear directionality (main ring). For amatoxins, this ring is the peptide ring (macrolactam), where the direction is defined by the sequence N $\rightarrow$ C $_{\alpha}$ $\rightarrow$ carbonyl-C. Because of this directionality, the main ring has two distinct sides, and the position of the second cycle with respect to the main ring defines two distinct isomers. In our previous study,[29] we suggested the term ansamers for this type of isomerism, with P-ansamer denoting one option and M-ansamer the other. To assign the stereochemical descriptor (M or P configuration), the CIP (Cahn-Ingold-Prelog) rules can be followed.[29] One proceeds as follows (Figure 1.a):

1. Identify the main ring and its directionality.
2. Identify the bridge-head atom α where the second cycle branches from the main ring.
3. Identify the leading atom L in the second cycle.
4. If looking along direction $L \rightarrow \alpha$,
   - the main ring proceeds clockwise, the structure is a P-ansamer
   - the main ring proceeds anti-clockwise, the structure is a M-ansamer.

Because, the second cycle always has two bridgeheads, one has two choices in step 2, but both choices lead to the same result. In amatoxins, the second cycle is the tryptathionine

bridge, and the *P*-ansamer is often described as "bridge up", whereas the *M*-ansamer is described as "bridge down". This becomes understandable if one considers an equivalent procedure to identify the ansamers which uses a "left-hand rule" (Figure 1.a)

1. Identify the main ring and its directionality.
2. Curve the fingers of the left-hand in the directionality of the main ring. The direction of the thumb defined "up".
3. If the second cycle and the thumb are located
   - on the same side, the structure is a *P*-ansamer
   - on different sides, the structure is a *M*-ansamer.

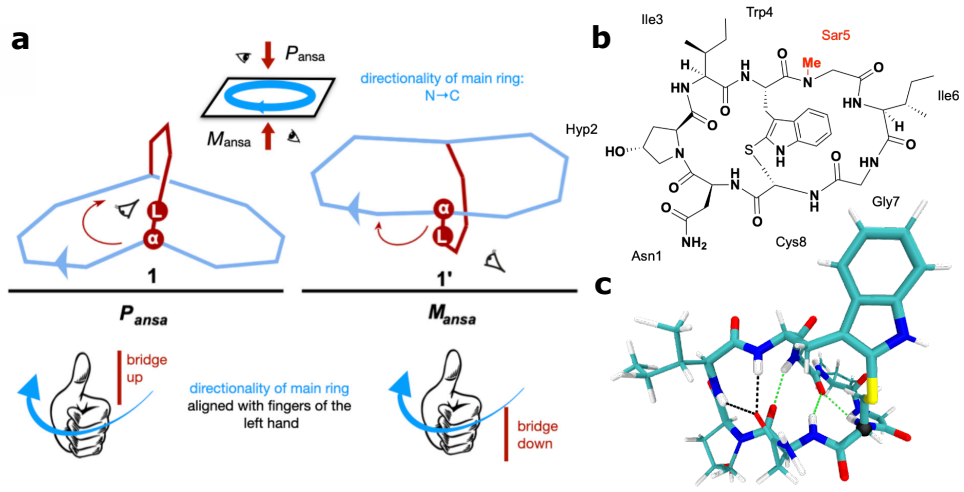

Figure 1: a) Definition of the ansamers P_{ansa} and M_{ansa} (Figure adapted from Ref. 29). b) Chemical structure of Gly5Sar-amanullin. c) Crystal structure of P_{ansa}-amanullin (CCDC deposition numbers: 1128063[41]). The structure is coloured according to atom type: *cyan:* carbon; *white:* hydrogen; *red:* oxygen; *blue:* nitrogen; *yellow:* sulphur. The C_α-atom of Cys8 is highlighted as black sphere. Hydrogen bonds are shown as dotted lines and coloured green if Gly5 is involved.

So far, only the *P*-ansamers of amatoxins have been isolated from mushrooms,[16] but in the laboratory we could also synthesise *M*-ansamers.[24,29]

We synthesised Gly5Sar-amanullin (Figure 1.b) using our previously developed strategy:[24,29] the iodine-mediated tryptathionine bridge formation and the bicycle ring-closure

between Hyp2 and Ile3. We verified the product by HPLC-HRMS, ^{1}H-NMR spectroscopy and UV-VIS spectroscopy. With our current protocol, we obtained exclusively one of the two possible ansamers, and the UV-VIS spectrum, CD spectrum and NMR NOE data suggest that it is the M-ansamer of Gly5Sar-amanullin (see Supplementary Information, sections 1 and 2).

The M-ansamer has two populations in slow exchange

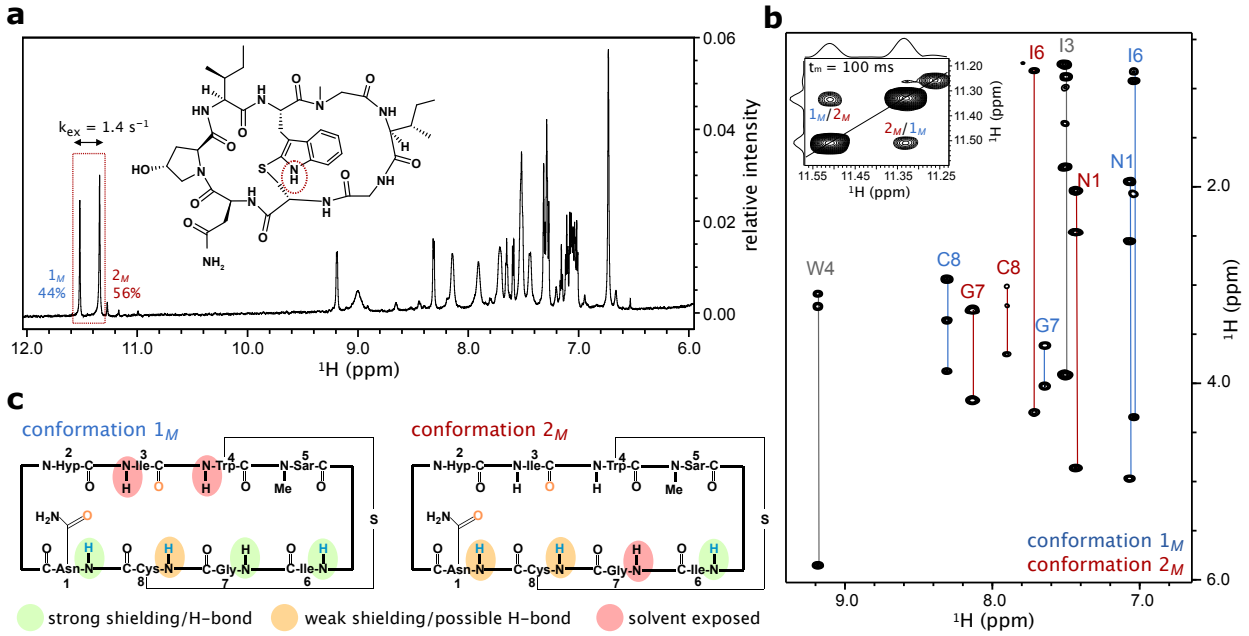

Figure 2: Experimental evidence for the conformational exchange in M_{ansa}-Gly5Sar-amanullin. a) Amide region of the ^{1}H-NMR spectrum of Gly5Sar-amanullin. Two signals are visible for the indole amine proton (red box), suggesting two conformations of the peptide. The exchange rate k_{ex} = 1.4 s^{-1} was measured by EXSY NMR. The rate constants were $k_{1_M \rightarrow 2_M}$= 0.84 s^{-1} and $k_{2_M \rightarrow 1_M}$ = 0.54 s^{-1}. b) The ^{1}H-^{1}H-TOCSY NMR spectrum of M_{ansa}-Gly5Sar-amanullin shows two sets of amide correlation signals for Asn1, Ile6, Gly7 and Cys8. The signals were assigned to either conformation 1_M (blue labels) or conformation 2_M (red labels). The inset shows the diagonal peaks of the two indole (-NH) proton signals with chemical exchange cross peaks in the TOCSY spectrum. c) Strongly shielded amides with larger temperature correlation coefficients ($\Delta\delta$HN/ΔT > -3.0 ppbK^{-1}) suggesting H-bonding are highlighted in green. Solvent exposed amides with small temperature correlation coefficients ($\Delta\delta$HN/ΔT < -4.6 ppbK^{-1}) are highlighted in red and amides with weak shielding/H-bonding are shaded in orange.

The ^{1}H-NMR spectrum of the M-ansamer of Gly5Sar-amanullin showed two distinct

peaks for the amine of the tryptophan side chain, suggesting two different conformers for the M-ansamer: 1_M and 2_M (Figure 2.a). From the integral under the two peaks in the 1D spectrum, we estimated the relative populations to be 37% for 1_M and 62% for 2_M at 298 K. The spectrum also shows a very small third peak corresponding to less than 1% of the population. The peaks in the ^{1}H-NMR spectrum correspond to only a single chemical species, suggesting that 1_M and 2_M represent different conformers of the M-ansamer (Note that the subscript M in 1_M and 2_M stands for M-ansamer and not for magnetization.)

The ^{1}H-^{1}H-TOCSY spectrum, two sets of amide correlation signals were observed for Asn1, and the amino acids in the "eastern" ring of the bicycle (Ile6, Gly7 and Cys8). Additionally, we observe an exchange peak between the two indole (-NH) proton peaks (Figure 2.b). The two dominant peaks exchanged with a rate of $k_{\text{ex}} = 1.381\,\text{s}^{-1}$ in the ^{1}H-^{1}H-EXSY spectrum at 298 K.The exchange rate is defined as $k_{\text{ex}} = k_{1_M \to 2_M} + k_{2_M \to 1_M}$, where $k_{1_M \to 2_M}$ is the rate from 1_M to 2_M, and $k_{2_M \to 1_M}$ is the rate for the reverse reaction. We measured $k_{1_M \to 2_M} = 0.84\ \text{s}^{-1}$ and $k_{2_M \to 1_M} = 0.54\ \text{s}^{-1}$ at 298 K. From these rates, we can estimate the populations to be 39% for 1_M and 61% for 2_M, which is in excellent agreement with the estimates from the 1D-spectrum. On the other hand, a conformational transition that occurs on a timescale of seconds is unusual for a cyclic peptide, which (at least in MD simulations) have conformational equilibration times in the range of 100 ns to several microseconds[30–33]

For both populations, we extracted NOE distances, and we determined the shielding of the amide protons by a variable-temperature NMR experiment (Figure 2.c). The NOE distance set for 1_M contains 67 upper distance bounds, that of 2_M contains 41 upper distance bounds. Of these, 11 distances appear in both sets. For 1_M, we could additionally measure the $^3J_{\text{H}^\text{N}\text{H}^\alpha}$-coupling constants which was not possible for 2_M due to the larger line widths of the amide proton signals. (see Supplementary Table 3).

Characterisation of M_{ansa}-Gly5Sar-amanullin

Next, we set out to identify the three-dimensional structure of 1_M and 2_M using classical molecular-dynamics (MD) simulations. The exchange rate of $k_{\text{ex}} = 1.381\ \text{s}^{-1}$ indicates that, at room temperature, the conformational dynamics is slow compared to the timescales that are accessible by classical MD simulations. The first challenge therefore is to explore the conformational space. Starting form two different structures, we simulated M_{ansa}-Gly5Sar-amanullin at 300 K, 400 K, 500 K and 700 K for 24 μs, respectively. The molecule was solvated in dimethyl sulfoxide (DMSO), which was modelled explicitly. The simulations at 400 K and higher temperatures do not represent faithful representations of the molecule at high temperatures but solely serve to explore the conformational space. (See Supplementary Information section 3 for computational details.)

Cis-trans isomerism of non-proline residues

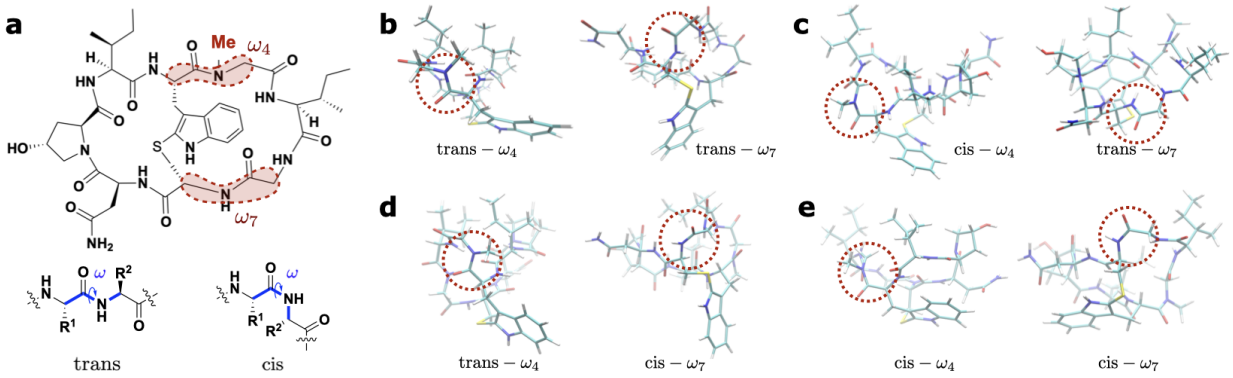

Figure 3: cis-trans isomerism in M_{ansa}-Gly5Sar-amanullin (a) resulting in four different configurations (b-d). a) chemical structure of Gly5Sar-amanullin with ω_4 and ω_7 highlighted. Below, the general 'cis' and 'trans' configuration of ω are shown for an arbitrary peptide group. ω highlighted in blue, is defined according to IUPAC: $C_{\alpha,i}$– carbonyl-C_i-N_{i+1}-$C_{\alpha,i+1}$.[45] b)-d) For each configuration, the determining (ω_4,ω_7)-torsion angles are shown in the structures (red circles): b) (trans-ω_4, trans-ω_7); c) (cis-ω_4, trans-ω_7); d) (trans-ω_4, cis-ω_7); e) (cis-ω_4, cis-ω_7). Each structure is coloured according to atom type: *cyan:* carbon; *white:* hydrogen; *red:* oxygen; *blue:* nitrogen; *yellow:* sulphur.

At 500 K, the typical, sterically-allowed regions of the Ramachandran plot of each of the residues are explored, and we observe transitions between the two starting conformations.

Additionally, we observe cis-trans isomerisation in several ω-torsion angles (Figure 3), specifically ω_4 (between Trp4 and Sar5), ω_5 (between Sar5 and Ile6), ω_7 (between Gly7 and Cys8), and ω_8 (between Cys8 and Asn1). Following the IUPAC definition,[45] ω_i is the torsion angle defined by $C_{\alpha,i}-$ carbonyl-C_i- $N_{i+1} - C_{\alpha,i+1}$. The torsion angle ω_1 (between Ans1 and Hyp2) samples a very broad distribution in the cis-configuration, but does not fully transition to the trans-configuration. The flexibility of ω_1 at high temperatures, however, is not surprising, because Hyp2 is a hydroxylated proline-variant and the peptide group prior to a proline-residue has a relatively small barrier for this isomerisation compared to regular peptide group.[46,47] Typical isomerisation barriers for a peptide group prior to a proline-residue are about 90 kJ·mol^{-1} Apart from ω_1, the four torsion angles which show cis-trans isomerisation stand out, because they are close to the tryptathionine bridge.

We simulated M_{ansa}-Gly5Sar-amanullin at 700 K to test whether ω_2, ω_3, and ω_6 could also exhibit cis-trans isomerization. This was not the case. Even at this high temperature, the three torsion angles remained in the trans-configuration.

When cooling the ensemble from 500 K to 400 K, we keep observing cis-trans transitions in ω_4 (between Trp4 and Sar5) and ω_7 (between Gly7 and Cys8). ω_5 (between Sar5 and Ile6) and ω_8 (between Cys8 and Asn1) do not show any transitions and only sample the trans-configuration. Cooling the ensemble further to 300 K, we keep observing occasional cis-trans transitions in ω_4. For ω_7, both cis- and trans-configurations are present in the ensemble, but in different trajectories. We do not observe any transitions between these two configurations at room temperature during our simulations. (See Supplementary Figures 6-8 for the Ramachandran plots and the distributions of the ω-torsion angles at all simulated temperatures as well as the time series of ω_4 at 300 K.)

In the simulated ensemble at 300 K, four different configurations are present (Figure 3): (trans-ω_4, trans-ω_7), (trans-ω_4, cis-ω_7), (cis-ω_4, trans-ω_7), and (cis-ω_4, cis-ω_7). (trans-ω_4,

trans-ω_7) is the expected conformation and occurs in the majority of the 24 trajectories. (cis-ω_4, trans-ω_7) occurs in two trajectories, and (trans-ω_4, cis-ω_7) and (cis-ω_4, cis-ω_7) each occur in one trajectory (see Supplementary Table 5). Apart from short excursion from (trans-ω_4, trans-ω_7) to (cis-ω_4, trans-ω_7), we don't observe transitions between the four configurations. Note that we do not observe any cis-trans isomerisation for ω_1, i.e. in the peptide bond which precedes the proline-variant Hyp2.

The chemical shifts of the C_β proton in Hyp2 of M_{ansa}-Gly5Sar-amanullin are similar to those in the M-asamer of amanullin.[29] It thus seem likely that ω_1 is in the cis-configuration, which agrees with our MD results. Unfortunately, the configuration of ω_4 and ω_7 cannot be unambiguously assigned from our NMR data. However, cis-trans isomerisation in peptides with N-methylated amino acids and particular in peptides with sarcosine have been reported previously.[48] Likewise cis-trans isomerisation in strained cyclic peptides without N-methylated amino acids are known.[49] The exchange rates for the cis-trans isomerisation reported in Ref. 49 are on the order of 1 s^{-1} and are thus in the same range as the exchange rate between 1_M and 2_M. Overall, it seems possible that 1_M and 2_M correspond to two different configurations of the peptide backbone M_{ansa}-Gly5Sar-amanullin rather than to two different conformations within the (trans-ω_4, trans-ω_7)-ensemble.

Comparison of MD structure and NMR data for the M-ansamer

We compared the four (ω_4, ω_7)-configurations to our NMR data. The (trans-ω_4, trans-ω_7)-MD ensemble shows an almost perfect fit to the NOE upper distance bounds for 1_M (Figure 4.d). We can only identify two small violations for the 67 NOE distances. The corresponding distances are shown as pink lines in Figure 4.c. By contrast, the other three configurations show considerably more violations of the NOE upper distance bounds for 1_M, in particular for main chain-main chain and the main chain-side chain distances (Supplementary Figure 9).

Furthermore, the (trans-ω_4, trans-ω_7)-configuration is stabilised by hydrogen bonds from

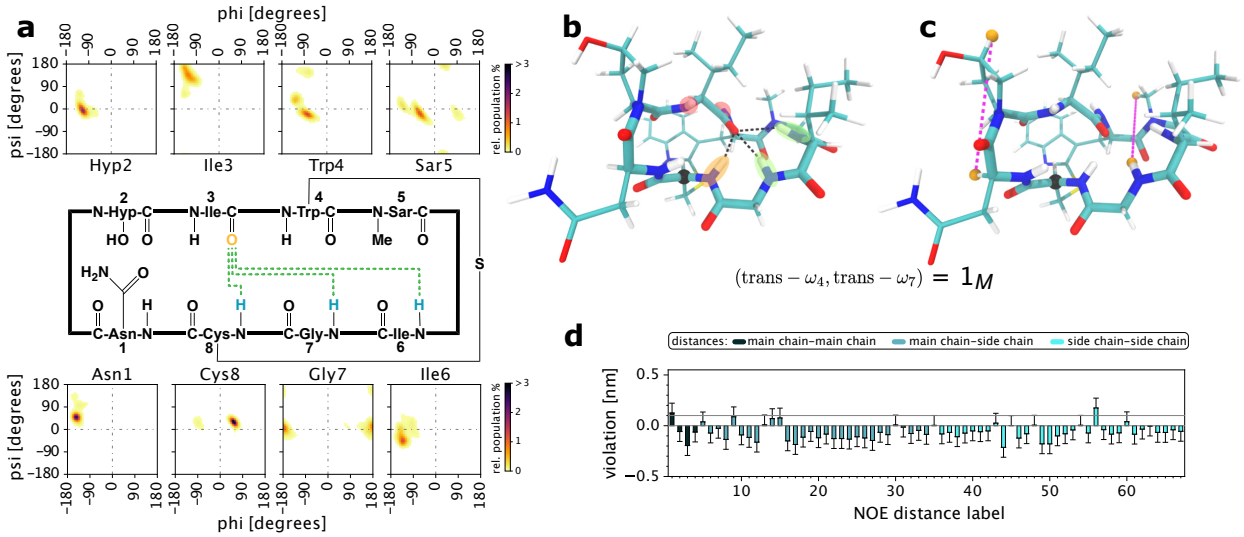

Figure 4: Conformation M_{ansa}-Gly5Sar-amanullin extracted from the (trans-ω_4, trans-ω_7)-MD ensemble at 300 K. (a) Hydrogen bond pattern and Ramachandran plots. *green dashed line:* hydrogen bonds with $\geq$ 20% population in the MD ensemble. The colourmap in the Ramachandran plots shows the total probability density within the (trans-ω_4, trans-ω_7)-ensemble. (b,c) MD structure for (trans-ω_4, trans-ω_7)-Gly5Sar-amanullin showing the highest-populated hydrogen bonds (b, black dashed line) or the NOE violations (d, purple dashed lines). The structures are coloured according to atom type. *cyan:* carbon; *white:* hydrogen; *red:* oxygen; *blue:* nitrogen; *yellow:* sulphur. The C_α-atom of Cys8 is highlighted as black sphere. In b), the amides of Ile3, Trp4, Ile6, Gly7 and Cys8 are additionally coloured according to their NMR shielding (Figure 2.c). (d) Violations of the NOE upper distance bounds from the experimental structure 1_M shown the for the (trans-ω_4, trans-ω_7)-MD ensemble at 300 K. For each NOE distance, the violation is shown as average (bar) and standard deviation (errorbar) over the (trans-ω_4, trans-ω_7)-MD ensemble.

the amide protons of Ile6, Gly7 and Cys8 to the carbonyl oxygen of Ile3 (Figure 4.a). These hydrogen bonds agree well with the solvent exposure determined from variable-temperature NMR experiments (Figure 2.c and Figure 4.b). The hydrogen-bond pattern of (trans-ω_4, cis-ω_7)-configuration shows a similar agreement with the variable-temperature NMR experiments, but the configurations in which ω_4 is in the cis-configuration are stabilized by hydrogen bond patterns that are not consistent with these data (Supplementary Figures 10-11).

$^3J_{\mathrm{H_N H_\alpha}}$-coupling constants depend on the H^N-C-C-H^α torsion angle, which related ϕ-backbone torsion angle by a shift of about 60° (depending on the bond angles at the two carbon atoms). These coupling constants can thus be used to gauge the conformation of the the H^N-C-C-H^α torsion angle and the closely related ϕ-backbone angles. (ϕ_i is defined by the backbone atoms C_{i-1}, N_i, $\mathrm{C}_{i[\alpha]}$, C_i, see Ref.[45]). However, the comparison between simulated and experimental $^3J_{\mathrm{H_N H_\alpha}}$-coupling is notoriously difficult , because the Karplus curve which links the ϕ-torsion angles to the $^3J_{\mathrm{H_N H_\alpha}}$ constant is highly-nonlinear and sensitive to the parametrization of the curve. Consequently, inaccuracies of in the potential energy of the simulations can lead to shifts in the predicted $^3J_{\mathrm{H_N H_\alpha}}$ by more than 1 Hz.[50,51] The comparison of the four configurations to the $^3J_{\mathrm{H_N H_\alpha}}$-coupling constants for 1_M confirms that the cis-ω_4-configurations are not consistent with the NMR data of 1_M. Both trans-ω_4-configurations agree equally well with the $^3J_{\mathrm{H_N H_\alpha}}$-coupling constants for 1_M . We tested different parametrisations of the Karplus curve[52,53] and accounted for the sensitivity of the estimated $^3J_{\mathrm{HNC^\alpha H}}$-coupling constants with respect to inaccuracies of the potential energy function by shifting the values of H^N-C-C-H^α-torsion angle by +10° and -10° (Supplementary Figure 12). Overall, (trans-ω_4, trans-ω_7)-configuration agrees best with the NMR data for 1_M, and we assign this configuration (Figure 4) to the corresponding 1_M signal in the NMR data.

For 2_M, we have less NMR data, and the comparison to the four configurations unfortunately remains inconclusive. All four configurations show violations of the NOE upper distance bounds for 2_M (Supplementary Figure 9). However, the trans-ω_7-configurations

show fewer violations than the cis-ω_7-configurations. Specifically, they do not have any violations in the critical main-chain-main-chain distances. However, none of the four configurations showed a hydrogen bond pattern that is consistent with the shielding derived of the amide protons in 2_M as measured in the variable-temperature experiments (Supplementary Figure 11). Overall, 2_M seems to be consistent with a trans-ω_7-configuration, but a definite assignment is not possible.

Thus, from experimental data it seems likely that ω_7 is in the trans-configuration in 1_M as well as in 2_M. Since we are confident that ω_4 is in the trans-configuration in 1_M, there are two possible structural explanations for the exchange between 1_M and 2_M. The exchange can either correspond to a cis-trans isomerisation in ω_4 or to a conformational transition within the (trans-ω_4, cis-ω_7)-configuration.

Conformational ensemble of the (trans,trans)-configuration

We analyzed the ensemble of the (trans,trans)-configuration of M_{ansa}-Gly5Sar-amanullin at 300 K in more detail (Supplementary Figure 13). To identify conformations within this ensemble, we performed a dimensionality reduction based on the conformational dynamics of all backbone torsion angles (time-independent component analysis[54,55]) and clustered in the reduced space using the density-based cluster algorithm common-nearest-neighbour clustering (CommonNN).[56–59] We obtained 5 clusters (c1-c5, Figure 5.a). Figure 5.b shows the distribution of the ensemble in the reduced space of four time-independent components (TICs, see also Supplementary Figure 14). Figure 5.c shows how the five clusters are located within this space.

We determined the timescale of the conformational exchange between these five clusters using a core-set Markov model[58–61] (Figure 5.a). We find that three clusters (c1, c2 and c5) are well-connected on the timescale of the MD simulation, whereas we do not observe sufficiently many transitions to clusters c3 and c4 to include them in then in the Markov model.

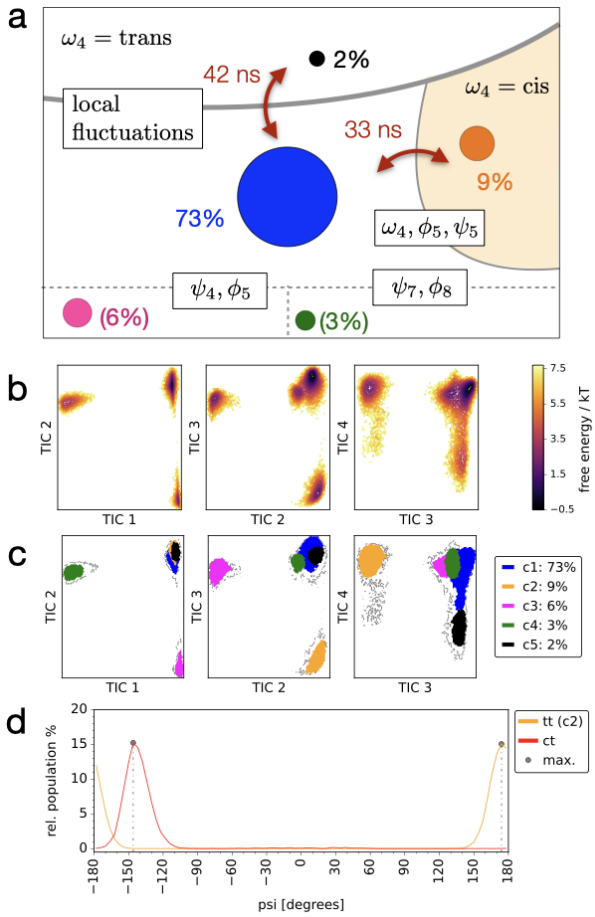

Figure 5: Conformational dynamics of the (trans-ω_4, trans-ω_7)-configuration **a**: kinetic model derived from a core-set Markov model. Clusters c1 to c5 are represented as coloured circles (blue: c1, orange: c2, pink: c3, green: c4, black: c5). Cluster populations are given in % next to the circles. Gray line represent free-energy barriers for the conformational exchange between clusters or groups of clusters. The associated equilibration timescales are shown in red next to the double arrors. White boxes show the torsion angles involved in a particular conformational exchange. **b**: dimensionality reduction by time-independent component analysis: free energy as a function of the first four time-independent components; **c**: CommonNN-clustering in the space of the time-independent components; **d**: distribution of ψ_5 in the cluster c2 and in the (cis-ω_4, trans-ω_7)-configuration

The most populated cluster is c1 (population 73%; blue circle in Figure 5.a) and its structure is shown Figure 4.b. Cluster c5 (population 2%; black circle in Figure 5.a) represents local fluctuations around this structure that do not involve any major transitions in the backbone torsion angles. These local fluctuations equilibrate on a timescale of about 42 ns (Supplementary Figure 15). In both c1 and c5, the ω_4-torsion angles remain in the trans configuration.

By contrast, cluster c2 (population 9%; orange circle in Figure 5.a) represents short excursions into the cis-configuration of ω_4, i.e. the ω-torsion angle between Trp4 and Sar5. This transition is coupled to a transition in the ϕ- and ψ-backbone torsion angle of Sar5. However, the resulting (cis-ω_4,trans-ω_7)-configurations are only stable on a timescale of 33 ns. This timescale is at variance with the observation that the (cis-ω_4,trans-ω_7)-configurations is stable over at least 1 μs in the trajectories discussed above. It seems likely that the excursion into the cis-configuration of ω_4 in cluster c2 are recrossing events.[62] This means, the molecule crosses the barrier between cis- and trans-configurations, but does not fully reach free energy minimum of the (cis,trans)-configuration and instead quickly returns to (trans,trans)-configuration. This interpretation is substantiated by the fact that the distribution of ψ_5 in the (cis,trans)-configuration is slightly shifted with respect to the ψ_5-distribution in the (trans,trans)-configuration. That is, to fully reach a stable (cis,trans)-configuration, the ψ_5-torsion angle needs to shift by about 40° from 174° in cluster c2 to -146° in the (cis,trans)-ensemble (Figure 5.d). It should be noted, however, that the torsion angles are periodic, so the shift is effectively 40°.

Cluster c3 (population 6%; pink circle in Figure 5.a) represents a transition from cluster c1 in the ψ-torsion angle of Trp4 and the ϕ-torsion angle in Sar5, where the intermediate ω_4 remains in the trans-configuration. Cluster c4 (population 3%; green circle in Figure 5.a) represents a transition from cluster c1 in the ψ-torsion angle of Gly7 and the ϕ-torsion angle in Cys8, where the intermediate ω_7 remains in the trans-configuration.

Note though that the transitions between c1 and c3 and c4, respectively, are not sampled

sufficiently. Thus, the relative populations are not well-converged and are denoted in brackets. (See Supplementary Figure 16-17 for the distributions of the residue-specifc ω-backbone torsion angles as well as the hydrogen bonds in the clusters c1-c5.)

Characterisation of P_{ansa}-Gly5Sar-amanullin

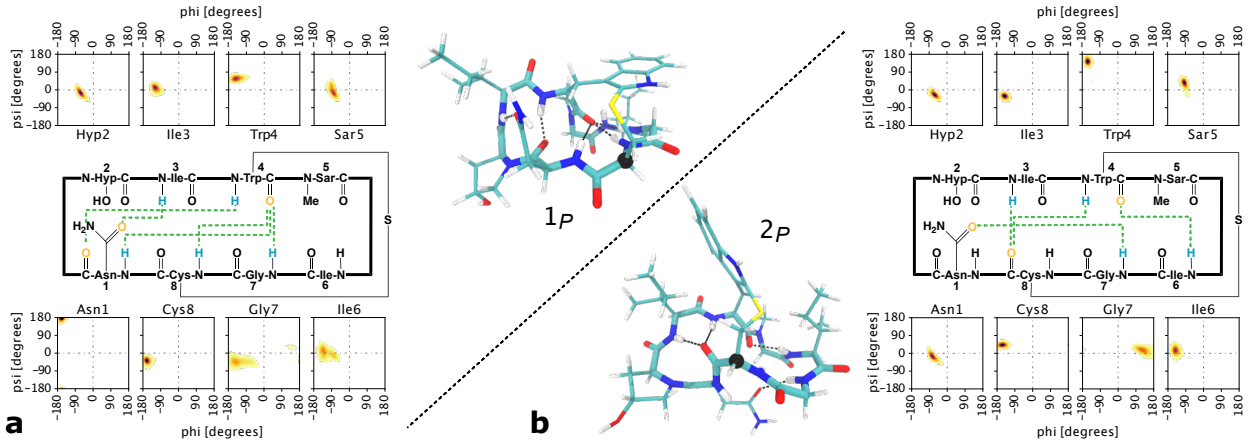

Figure 6: Conformation 1_P (a) and 2_P (b) of P_{ansa}-Gly5Sar-amanullin extracted from MD simulations at 300 K. For each conformation, the hydrogen bond pattern, Ramachandran plots and structure are shown. Hydrogen bonds with a population $\geq 20\%$ within the MD ensemble of the respective conformation are depicted as *green dashed lines* in the scheme and *black dashed lines* in the structure. The structures are coloured according to atom type. *cyan:* carbon; *white:* hydrogen; *red:* oxygen; *blue:* nitrogen; *yellow:* sulphur. The C_α-atom of Cys8 is highlighted as black sphere.

We explored the conformational space of P-ansamer of Gly5Sar-amanullin in a similar manner as for the M-ansamer: we simulated the molecule at high temperatures (up to 800 K) and stepwise cooled the ensemble to 300 K. In contrast to M_{ansa}-Gly5Sar-amanullin, we do not observe any cis-trans isomerisation in the backbone of the P-ansamer of Gly5Sar-amanullin at 300 K. All ω-torsion angles are in trans-configuration, which is line with the previously published crystal structure of P-amanullin.[29] However, when cooling the ensemble to 300 K, we find two different conformations of P_{ansa}-Gly5Sar-amanullin: 1_P (Figure 6.a) and 2_P (Figure 6.b). In total, we have 36 μs MD trajectories of 1_P at temperatures between 300 K and 340 K, and 50 μs MD trajectories of 2_P at 300 K, but we do not observe any transitions

between the two conformations. That is, the conformational exchange between these two structures is slow in the timescale of the MD simulations. 1_P and 2_P differ in the conformation of the backbone torsion angle ϕ and ψ of most residues and in the intramolecular hydrogen bond pattern (Supplementary Figure 18). In 1_P, the intramolecular hydrogen bond network mostly affects the left cyclic subunit, and consequently the right cyclic subunit is somewhat flexible, in particular in the backbone of Ile6 and Gly7. By constrast, the hydrogen bond network in 2_P affects all regions of the peptide ring and this conformer is more rigid than 1_P.

Comparison between amanullin and Gly5Sar-amanullin

We previously published the crystal structures of both ansamers of amanullin.[29] Figure 7 compares these structures to the corresponding structures of Gly5Sar-amanullin, which we obtained from our simulations. For Gly5Sar-amanullin, we here only consider the (trans,trans)-configuration.

The M-ansamer of amanullin is stabilized by hydrogen bonds from amide hydrogens of Ile6, Gly7 and Cys8 across the peptide ring to the carbonyl group of Ile3 (Figure 7.a). The amide hydrogen of Gly5 is solvent exposed, and is not involved in stabilizing the structure. Consequently, methylating this position has little effect on the conformation of the molecule. The (trans,trans)-configuration of M-Gly5Sar-amanullin exhibits the same hydrogen bond patterns as M-amanullin (Figure 7.b), and have the same backbone structure (within the variation due to thermal vibrations)(Figure 7.c).

By contrast, the P-ansamer of amanullin is stabilized by a hydrogen-bond network, which includes a hydrogen bond from the amide hydrogen of Gly5 across the peptide ring to the carbonyl oxygen Asn1 (Figure 7.d). This hydrogen bond cannot be formed in P-Gly5Sar-amanullin, and different hydrogen bond patterns arise. Instead of one conformational isomer in P-amanullin, we find two major conformations in P-Gly5Sar-amanullin. In the conformation 1_P, the hydrogen bond pattern is shifted by one residue compared to P-amanullin

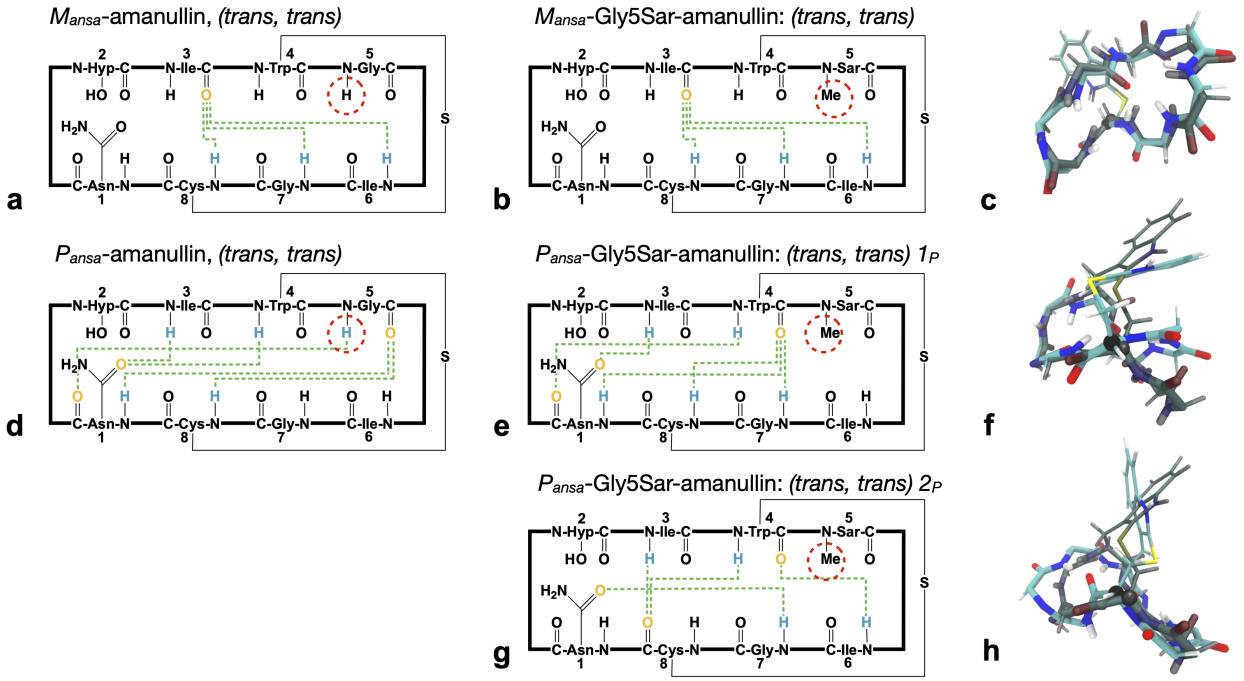

Figure 7: Comparison between the crystal structures for P_{ansa}- and M_{ansa}-amanullin (CCDC deposition numbers: 1128063,[41] 2153904[29]) and the conformations 1_M, 1_P and 2_P from our MD simulations on Gly5Sar-amanullin. (a-g) Hydrogen bond schemes for the crystal structures and the structures from MD. Hydrogen bonds are depicted as green dotted lines between the donor atom (blue) and the acceptor atom (orange). (c,f,h) Superposition of the Gly5Sar-amanullin conformations (coloured) 1_M (c), 1_P (f) and 2_P (h) with the respective amanullin crystal structure (grey). The structures are coloured according to atom type: carbon : cyan, hydrogen : white, oxygen : red, nitrogen : blue, sulphur : yellow. All structures have been fitted on the backbone of the residues Gly7, Cys8, Asn1, Hyp2 and Ile3.

(Figure 7.e). The Gly5-Ans1 hydrogen bond is replaced by Trp4-Ans1 hydrogen bond. And instead of forming hydrogen bonds to the carbonyl oxygen of Gly5, the amide protons of Asn1 and Cys8 now form hydrogen bonds to Trp4. The conformation 2_P is stabilized by a hydrogen bond pattern (Figure 7.g) that is completely different from the hydrogen bonds of P-amanullin. Consequently, the backbone structure of either conformation of P-Gly5Sar-amanullin differs from the conformation of P-amanullin (Figures 7.f and 7.h).

To assess possible differences in the physico-chemical properties of the five structures in Figure 7, we calculated their surface accessible area (SASA) and decomposed this area into a hydrophilic and a hydrophobic contribution (Table 1). However, the various structures

showed only small differences in these properties.

Table 1: Solvent accessible surface area (SASA), hydrophobic and hydrophilic fraction of the SASA

			SASA [nm^2]	hydrophilic	hydrophobic
amanullin					
M ansamer	(trans-ω_4,trans-ω_7)		9.22	31 %	69 %
P ansamer	(trans-ω_4,trans-ω_7)		10.05	32 %	68 %
Gly5Sar-amanullin					
M ansamer	(trans-ω_4,trans-ω_7)		9.89±0.15	37 %	63 %
P ansamer	(trans-ω_4,trans-ω_7)	1_P	9.7±0.38	32 %	68 %
P ansamer	(trans-ω_4,trans-ω_7)	2_P	9.3±0.28	34 %	66 %

Conclusion and outlook

We combined NMR experiments and MD simulations to elucidate the influence of N-methylation on the structural ensemble of an amatoxin, specifically we compared Gly5Sar-amanullin and amanullin. Due to their bicyclic structure, amatoxins can form two different ansamers, and the effect of N-methylation is different in the two ansamers.

In the P-ansamer of Gly5Sar-amanullin, the methyl group prevented a hydrogen bond that is present in P_{ansa}-amanullin and two new conformations could arise. The exchange of these two new conformations was slow on the timescale of the MD simulations (microseconds).

By contrast, M_{ansa}-amanullin does not have a hydrogen-bond to the amide-proton of Gly5, and it is overall very rigid. Thus, one could have expected that methylation of Gly5 has little effect on the structure of this ansamer. Yet, we found two populations in the NMR experiments which exchanged with a rate of 1.38 s^{-1}.

The MD-data showed cis-trans isomerization in two ω-torsion angles of M_{ansa}-Gly5Sar-amanullin: one involved the methylated amide (ω_4), the other was located on the opposite site of the tryptathionine bridge (ω_7). We could assign the (trans-ω_4, trans-ω_7)-configuration to the 1_M signal in the NMR data. The 2_M signal could not be assigned unambiguously

to an MD-structure. However, we could rule out that 2_M is a cis-ω_7-configuration. Since the MD simulations of the (trans-ω_4, trans-ω_7)-configuration showed short excursions to the (cis-ω_4, trans-ω_7)-configuration, it seems likely that the exchange between the two NMR signals corresponds to a cis-trans isomerization

Our results show that, even though amatoxins have a relatively rigid scaffold, methylation of the backbone amides can have varied and sizeable effects on their overall structure. N-methylation can lower the rotational barrier of the corresponding ω-torsion angle and can give rise to thermal cis-trans isomerization on the timescale of seconds. And even within a given configuration, the introduction of a methyl-group prohibits certain intramolecular hydrogen bonds and generates new conformations.

Methods

Computational and experimental methods are reported in the Supplementary Information.

Acknowledgement

This research has been funded by Deutsche Forschungsgemeinschaft (DFG) through grant RTG 2473 Bioactive Peptides - Project ID 392923329 - Project C01. SFB 1349 Fluorine-Specific Interactions - Project ID 387284271, Project A05. We thank the Zentraleinrichtung für Datenverarbeitung (ZEDAT) of Freie Universität Berlin for computing time. We also thank the NMR Messzentrum at the Institute of Chemistry at TU Berlin for the use of their NMR spectrometers and especially Samantha Voges for assistance with spectra acquisition. Guiyang Yao thanks the Alexander von Humboldt Foundation for a postdoctoral fellowship and the National Natural Science Foundation of China (82204189).

Supporting Information Available

We provide the protocols (section 1) as well as spectroscopic evidence (section 2.1) for the synthesis of M_{ansa}-Gly5Sar-amanullin: reagents, solvents, chromatographic conditions, UV-VIS-, ^{1}H-NMR- and CD spectra.

We also provide all evidence from NMR experiments that indicates the presence of two long-living conformations for M_{ansa}-Gly5Sar-amanullin (1_M, 2_M, section 2.2): chemical shifts, amide temperature coefficients, $^{3}J_{\text{H}^{\text{N}}\text{H}^{\alpha}}$-coupling coefficients and inter-proton distances from ^{1}H-^{1}-NOESY-spectra (NOE distances)

Furthermore, we provide additional material for the characterisation of (1) the MD ensembles of M_{ansa}- and P_{ansa}-Gly5Sar-amanullin at different temperatures (2) the sub data sets for the 300 K MD ensemble of the M-ansamer incl. the assignment of the trajectories and (3) the clusters from sub data set 'tt' of the 300 K MD ensemble of M_{ansa}-Gly5Sar-amanullin (section 2.3) The characterisation involves backbone torsion angle (ϕ, ψ, ω) distributions, calculated $^{3}J_{\text{H}^{\text{N}}\text{H}^{\alpha}}$-coupling coefficients using different parameter sets for the Karplus equation, hydrogen bond populations and schemes with amides coloured according to expected solvent exposure, analysis of the inter-proton distances from the experimental NOE distances for 1_M and 2_M (tables and violation plots) and, for the clustering of the 'tt' sub data set: the eigenvalues and distributions for the time-independent components as well as the implied timescales for the constructed cs-MSM.

In sections 3 and 4, all computational and experimental methods used in this study are described and necessary parameters are provided. This involves the setup for the MD simulations of both ansamers of Gly5Sar-amanullin as well as the computational tools for their analysis (section 3). In addition, further details on the HPLC-MS, CD spectroscopy and on the NMR experiments (incl. proton assignments and variable temperature measurements) are given (section 4).

References

(1) Karlson-Stiber, C.; Persson, H. Cytotoxic fungi—an overview. *Toxicon* **2003**, *42*, 339–349.

(2) Wikipedia contributors, Amatoxin. 2022; `https://en.wikipedia.org/wiki/Amatoxin`, [Online; accessed 28 November 2022].

(3) Le Dare, B.; Ferron, P.-J.; Gicquel, T. Toxic effects of amanitins: Repurposing toxicities toward new therapeutics. *Toxins* **2021**, *13*, 417.

(4) Hallen, H. E.; Luo, H.; Scott-Craig, J. S.; Walton, J. D. Gene family encoding the major toxins of lethal Amanita mushrooms. *Proc. Natl. Acad. Sci.* **2007**, *104*, 19097–19101.

(5) Enjalbert, F.; Rapior, S.; Nouguier-Soulé, J.; Guillon, S.; Amouroux, N.; Cabot, C. Treatment of amatoxin poisoning: 20-year retrospective analysis. *J. Toxicol., Clin. Toxicol.* **2002**, *40*, 715–757.

(6) Walton, J. *The cyclic peptide toxins of Amanita and other poisonous mushrooms*; Springer, 2018.

(7) Block, S.; Stephens, R.; Barreto, A.; Murrill, W. Chemical identification of the Amanita toxin in mushrooms. *Science* **1955**, *121*, 505–506.

(8) Wieland, T.; Faulstich, H.; Fiume, L. Amatoxins, phallotoxins, phallolysin, and antamanide: the biologically active components of poisonous Amanita mushroom. *Crit. Rev. Biochem. Mol. Biol.* **1978**, *5*, 185–260.

(9) Wieland, T.; Faulstich, H. Fifty years of amanitin. *Experientia* **1991**, *47*, 1186–1193.

(10) Rudd, M. D.; Luse, D. S. Amanitin greatly reduces the rate of transcription by RNA polymerase II ternary complexes but fails to inhibit some transcript cleavage modes. *J. Biol. Chem.* **1996**, *271*, 21549–21558.

(11) Cramer, P.; Bushnell, D. A.; Kornberg, R. D. Structural basis of transcription: RNA polymerase II at 2.8 Ångstrom resolution. *Science* **2001**, *292*, 1863–1876.

(12) Brueckner, F.; Cramer, P. Structural basis of transcription inhibition by α-amanitin and implications for RNA polymerase II translocation. *Nat. Struct. Mol. Biol.* **2008**, *15*, 811–818.

(13) Kröncke, K.; Fricker, G.; Meier, P.; Gerok, W.; Wieland, T.; Kurz, G. alpha-Amanitin uptake into hepatocytes. Identification of hepatic membrane transport systems used by amatoxins. *J. Biol. Chem.* **1986**, *261*, 12562–12567.

(14) Meldolesi, J.; Pelosi, G.; Brunelli, A.; Genovese, E. Electron microscopic studies on the effects of amanitin in mice: liver and heart lesions. *Virchows Arch. path Anat.* **1967**, *342*, 221–235.

(15) Wikipedia contributors, a-amanitin. 2022; `https://en.wikipedia.org/wiki/ÎŠ-Amanitin`, [Online; accessed 28 November 2022].

(16) Pahl, A.; Lutz, C.; Hechler, T. Amanitins and their development as a payload for antibody-drug conjugates. *Drug Discov. Today: Technologies* **2018**, *30*, 85–89.

(17) Anderl, J.; Faulstich, H.; Hechler, T.; Kulke, M. In *Antibody-Drug Conjugates*; Ducry, L., Ed.; Humana Press: Totowa, NJ, 2013; pp 51–70.

(18) Matinkhoo, K.; Wong, A. A. W. L.; Hambira, C. M.; Kato, B.; Wei, C.; Müller, C.; Hechler, T.; Braun, A.; Gallo, F.; Pahl, A.; Perrin, D. M. Design, Synthesis, and Biochemical Evaluation of Alpha-Amanitin Derivatives Containing Analogs of the trans-Hydroxyproline Residue for Potential Use in Antibody-Drug Conjugates. *Chem. Eur. J.* **2021**, *27*, 10282–10292.

(19) Walton, J. D.; Hallen-Adams, H. E.; Luo, H. Ribosomal biosynthesis of the cyclic peptide toxins of Amanita mushrooms. *Biopolymers* **2010**, *94*, 659–664.

(20) Matinkhoo, K.; Pryyma, A.; Todorovic, M.; Patrick, B. O.; Perrin, D. M. Synthesis of the death-cap mushroom toxin α-amanitin. *J. Am. Chem. Soc.* **2018**, *140*, 6513–6517.

(21) Luo, H.; DuBois, B.; Sgambelluri, R. M.; Angelos, E. R.; Li, X.; Holmes, D.; Walton, J. D. Production of 15N-labeled α-amanitin in Galerina marginata. *Toxicon* **2015**, *103*, 60–64.

(22) Siegert, M.-A. J.; Knittel, C. H.; Süssmuth, R. A Convergent Total Synthesis of the Death Cap Toxin α-Amanitin. *Angew. Chem. Int. Ed.* **2019**,

(23) Lutz, C.; Simon, W.; Werner-Simon, S.; Pahl, A.; Müller, C. Total Synthesis of α-and β-Amanitin. *Angew. Chem. Int. Ed.* **2020**, *59*, 11390–11393.

(24) Yao, G.; Knittel, C. H.; Kosol, S.; Wenz, M. T.; Keller, B. G.; Gruß, H.; Braun, A. C.; Lutz, C.; Hechler, T.; Pahl, A. Iodine-Mediated Tryptathionine Formation Facilitates the Synthesis of Amanitins. *J. Am. Chem. Soc.* **2021**, *143*, 14322–14331.

(25) Wender, P. A.; Verma, V. A.; Paxton, T. J.; Pillow, T. H. Function-oriented synthesis, step economy, and drug design. *Acc. Chem. Res.* **2008**, *41*, 40–49.

(26) Zanotti, G.; Petersen, G.; Wieland, T. Structure-toxicity relationships in the amatoxin series: Structural variations of side chain 3 and inhibition of RNA polymerase II. *Int. J. Pept. Protein Res.* **1992**, *40*, 551–558.

(27) Schmitt, W.; Zanotti, G.; Wieland, T.; Kessler, H. Conformation of Different S-Deoxo-Xaa3-amaninamide Analogues in DMSO Solution as Determined by NMR Spectroscopy. Strong CD Effects Induced by βI, βII Conformational Change. *J. Am. Chem. Soc.* **1996**, *118*, 4380–4387.

(28) May, J. P.; Fournier, P.; Patrick, B. O.; Perrin, D. M. Synthesis, Characterisation, and In Vitro Evaluation of Pro2-Ile3-S-Deoxo-Amaninamide and Pro2-d-allo-Ile3-S-

Deoxo-Amaninamide: Implications for Structure–Activity Relationships in Amanitin Conformation and Toxicity. *Chem. Eur. J.* **2008**, *14*, 3410–3417.

(29) Yao, G.; Kosol, S.; Wenz, M. T.; Irran, E.; Keller, B. G.; Trapp, O.; Süssmuth, R. D. The occurrence of ansamers in the synthesis of cyclic peptides. *Nat. Commun.* **2022**, *13*, 6488.

(30) Razavi, A. M.; Wuest, W. M.; Voelz, V. A. Computational screening and selection of cyclic peptide hairpin mimetics by molecular simulation and kinetic network models. *J. Chem. Inf. Model.* **2014**, *54*, 1425–1432.

(31) Witek, J.; Wang, S.; Schroeder, B.; Lingwood, R.; Dounas, A.; Roth, H.-J.; Fouché, M.; Blatter, M.; Lemke, O.; Keller, B., et al. Rationalization of the membrane permeability differences in a series of analogue cyclic decapeptides. *J. Chem. Inf. Model.* **2018**, *59*, 294–308.

(32) Damjanovic, J.; Miao, J.; Huang, H.; Lin, Y.-S. Elucidating Solution Structures of Cyclic Peptides Using Molecular Dynamics Simulations. *Chem. Rev.* **2021**, *121*, 2292–2324.

(33) Linker, S. M.; Schellhaas, C.; Ries, B.; Roth, H.-J.; Fouché, M.; Rodde, S.; Riniker, S. Polar/apolar interfaces modulate the conformational behavior of cyclic peptides with impact on their passive membrane permeability. *RSC Adv.* **2022**, *12*, 5782–5796.

(34) Kessler, H. Conformation and Biological Activity of Cyclic Peptides. *Angew. Chem. Int. Ed.* **1982**, *21*, 512–523.

(35) Okumu, F. W.; Pauletti, G. M.; Vander Velde, D. G.; Siahaan, T. J.; Borchardt, R. T. Effect of restricted conformational flexibility on the permeation of model hexapeptides across Caco-2 cell monolayers. *Pharm. Res.* **1997**, *14*, 169–175.

(36) Witek, J.; Keller, B. G.; Blatter, M.; Meissner, A.; Wagner, T.; Riniker, S. Kinetic models of cyclosporin A in polar and apolar environments reveal multiple congruent conformational states. *J. Chem. Inf. Model.* **2016**, *56*, 1547–1562.

(37) Witek, J.; Mühlbauer, M.; Keller, B. G.; Blatter, M.; Meissner, A.; Wagner, T.; Riniker, S. Interconversion Rates between Conformational States as Rationale for the Membrane Permeability of Cyclosporines. *ChemPhysChem* **2017**, *18*, 3309–3314.

(38) Wang, C. K.; Swedberg, J. E.; Harvey, P. J.; Kaas, Q.; Craik, D. J. Conformational flexibility is a determinant of permeability for cyclosporin. *J. Phys. Chem. B* **2018**, *122*, 2261–2276.

(39) Corbett, K. M.; Ford, L.; Warren, D. B.; Pouton, C. W.; Chalmers, D. K. Cyclosporin Structure and Permeability: From A to Z and Beyond. *J. Med. Chem.* **2021**, *64*, 13131–13151.

(40) Tonelli, A. E.; Patel, D. J.; Wieland, T.; Faulstich, H. The structure of α-amanitin in dimethylsulfoxide solution. *Biopolymers* **1978**, *17*, 1973–1986.

(41) Shoham, G.; Rees, D. C.; Lipscomb, W. N.; Zanotti, G.; Wieland, T. Crystal and molecular structure of S-deoxo [Ile3] amaninamide: a synthetic analog of Amanita toxins. *J. Am. Chem. Soc.* **1984**, *106*, 4606–4615.

(42) Fosgerau, K.; Hoffmann, T. Peptide therapeutics: current status and future directions. *Drug Discov. Today* **2015**, *20*, 122–128.

(43) Hilimire, T. A.; Bennett, R. P.; Stewart, R. A.; Garcia-Miranda, P.; Blume, A.; Becker, J.; Sherer, N.; Helms, E. D.; Butcher, S. E.; Smith, H. C.; Miller, B. L. N-Methylation as a Strategy for Enhancing the Affinity and Selectivity of RNA-binding Peptides: Application to the HIV-1 Frameshift-Stimulating RNA. *ACS Chem. Biol.* **2016**, *11*, 88–94.

(44) Shoham, G.; Rees, D.; Lipscomb, W.; Zanotti, G.; Wieland, T. Crystal and molecular structure of S-deoxo [Ile3] amaninamide: a synthetic analog of Amanita toxins. *J. Am. Chem. Soc.* **1984**, *106*, 4606–4615.

(45) IUPAC-IUB Commission on Biochemical Nomenclature (CBN), Abbreviations and Symbols for the Description of the Conformation of Polypeptide Chains. 1969; `https://iupac.qmul.ac.uk/misc/noGreek/ppep3.html`, [Online; accessed 15 December 2022].

(46) Shibukawa, M.; Miyake, A.; Eda, S.; Saito, S. Determination of the cis–trans Isomerization Barriers of l-Alanyl-l-proline in Aqueous Solutions and at Water/Hydrophobic Interfaces by On-Line Temperature-Jump Relaxation HPLC and Dynamic On-Column Reaction HPLC. *Anal. Chem.* **2015**, *87*, 9280–9287.

(47) Schoetz, G.; Trapp, O.; Schurig, V. Determination of the cis-trans isomerization barrier of several L-peptidyl-L-proline dipeptides by dynamic capillary electrophoresis and computer simulation. *Electrophoresis* **2001**, *22*, 2409–2415.

(48) Matsoukas, J. M.; Moore, G. J. Proton magnetic resonance studies of angiotensin II conformation: cis-trans isomerism in sarcosine7-containing analogs. *Arch. Biochem. Biophys.* **1986**, *248*, 419–423.

(49) Mierke, D. F.; Yamazaki, T.; Said-Nejad, O. E.; Felder, E. R.; Goodman, M. Cis/trans isomers in cyclic peptides without N-substituted amides. *J. Am. Chem. Soc.* **1989**, *111*, 6847–6849.

(50) Christen, M.; Keller, B.; van Gunsteren, W. F. Biomolecular structure refinement based on adaptive restraints using local-elevation simulation. *J. Biomol. NMR* **2007**, *39*, 265–273.

(51) Li, S.; Elcock, A. H. Residue-Specific Force Field (RSFF2) improves the modeling of conformational behavior of peptides and proteins. *J. Phys. Chem. Lett.* **2015**, *6*, 2127–2133.

(52) Karplus, M. Contact electron-spin coupling of nuclear magnetic moments. *J. Chem. Phys.* **1959**, *30*, 11–15.

(53) Karplus, M. Vicinal proton coupling in nuclear magnetic resonance. *J. Am. Chem. Soc.* **1963**, *85*, 2870–2871.

(54) Pérez-Hernández, G.; Paul, F.; Giorgino, T.; De Fabritiis, G.; Noé, F. Identification of slow molecular order parameters for Markov model construction. *J. Chem. Phys.* **2013**, *139*, 07B604_1.

(55) Schwantes, C. R.; Pande, V. S. Improvements in Markov State Model Construction Reveal Many Non-Native Interactions in the Folding of NTL9. *J. Chem. Theory Comput.* **2013**, *9*, 2000–2009.

(56) Keller, B. G.; Daura, X.; van Gunsteren, W. F. Comparing geometric and kinetic cluster algorithms for molecular simulation data. *J. Chem. Phys.* **2010**, *132*, 02B610.

(57) Lemke, O.; Keller, B. G. Density-based cluster algorithms for the identification of core sets. *J. Chem. Phys.* **2016**, *145*, 164104.

(58) Lemke, O.; Keller, B. G. Common Nearest Neighbor Clustering—A Benchmark. *Algorithms* **2018**, *11*, 19.

(59) Kapp-Joswig, J.-O.; Keller, B. G. CommonNNClustering—A Python package for generic common-nearest-neighbour clustering. *bioRxiv* **2022**, 2022.11.28.518169.

(60) Buchete, N.-V.; Hummer, G. Coarse master equations for peptide folding dynamics. *J. Phys. Chem. B* **2008**, *112*, 6057–6069.

(61) Schütte, C.; Noé, F.; Lu, J.; Sarich, M.; Vanden-Eijnden, E. Markov state models based on milestoning. *J. Chem. Phys.* **2011**, *134*, 05B609.

(62) Eyring, H. The activated complex in chemical reactions. *J. Chem. Phys.* **1935**, *3*, 107–115.